Dielectric Relaxation Study of Some Novel Polymers for Nonlinear Optics

Werner Köhler,† Douglas R. Robello,* Craig S. Willand, and David J. Williams

Corporate Research Laboratories, Eastman Kodak Company, Rochester, New York 14650

Received November 8, 1990; Revised Manuscript Received February 15, 1991

ABSTRACT: Four novel polymers for nonlinear optics, two with the nonlinear chromophore in the side and two with the nonlinear chromophore in the main chain, were studied with dielectric relaxation spectroscopy. The results were compared with a host–guest system that contained the same chromophore as a monomeric dopant. In addition to the local relaxation modes of the nonlinear chromophores, present in all systems, for the two main-chain polymers an additional relaxation mode was found that is attributed to the global reorientation of the end-to-end vectors of the chains. The temperature dependence of the α relaxation, the conductivity, and the influence of interfacial polarization at the electrodes are discussed.

Introduction

The incorporation of organic chromophores with large second-order hyperpolarizabilities into glassy polymers and subsequent alignment in strong electric fields is a promising technique in the search for technologically useful materials for second-order nonlinear optics (NLO).[1,2] Large nonlinear susceptibilities, extremely fast response times due to the electronic origin of the nonlinear hyperpolarizabilities, and relatively simple processing techniques are attractive features of the technology and a considerable amount of research has been done in recent years.

Besides good mechanical and optical properties, like low scattering and absorption losses, the dynamics of the poling process itself and the long-term stability of the poled state are crucial factors for the utility of a particular material. Both issues are not yet very well understood.

Dielectric relaxation is a useful technique for studying the dynamic behavior of polymers, since it measures directly the motions of the ground-state dipole moments of the nonlinear chromophores. Furthermore, it can provide information about the ac and dc conductivity and about undesirable screening effects due to charge accumulation at partly blocking electrodes. Besides these more practical aspects, there is also a fundamental scientific interest in the investigation of the dynamics of polymers that contain very large densely packed dipole moments.

In this work, different polymers were investigated that all contained the same nonlinear optical chromophore, 4′-(dialkylamino)-4-(methylsulfonyl)azobenzene.[3] In this way, systematic changes that depend on the polymer and the method of chromophore incorporation could be investigated. The chemical structures of the polymers are shown in Figure 1, and the relevant physical data are summarized in Table I. For convenience, we adopt an abbreviation system for the materials, as follows:

DP is a host–guest system made by simply dissolving a monomeric chromophore in narrow molecular weight distribution polystyrene. The particular chromophore[3] was chosen because of its relatively high solubility in polystyrene.

SC1 is a side-chain methacrylic homopolymer in which the chromophore is covalently attached to a side chain via a flexible spacer unit.[4]

† Present address: Max-Planck-Institut für Polymerforschung, Ackermannweg 10, D-6500 Mainz, Germany.

Table I
Physical Properties of the NLO Polymers

	SC1	SC2	MC1	MC2	DP
ρ^a	1.28	1.20	1.18	1.20	
$\overline{M}_n \times 10^{-3}$ [b]	38.6	33.6	19.9	12.0	74.9
$\overline{M}_w \times 10^{-3}$ [b]	89.0	92.0	70.6	39.4	82.2
n^c	1.758	1.623	1.760	1.763	
$\epsilon_u{}^d$	4.3	3.8	4.0	3.9	2.55
T_g,[e] °C	100	109	60.5	92.4	91.0
$C_1{}^f$	13.7	15.5	11.8	11.8	11.6
C_2,[f] °C	54.3	65.4	46.4	42.9	46.3
$\log f_g{}^f$	−3.50	−4.19	−1.45	−2.05	−1.07
$f(T_g)^f$	0.032	0.028	0.037	0.037	0.037
$\alpha(T_g) \times 10^4{}^f$	5.8	4.3	7.9	8.6	8.1

[a] Density (in g/cm³) at room temperature. [b] Number- and weight-average molecular weights (in the case of DP for polystyrene host only), measured by SEC. [c] Refractive index at 632.8 nm. [d] Unrelaxed dielectric constant measured at 1 kHz and 23 °C. [e] Glass transition temperature measured by DSC. [f] Williams–Landel–Ferry parameters (see text).

SC2 is a (presumably) random copolymer with methyl methacrylate (MMA), which contains the same chromophore repeat unit as SC1. The mole ratio of chromophore to MMA is approximately 5:1.[4]

MC1 is a head-to-tail ("AB-type") polyester in which the chromopores are contained within the main chain and are separated by long, flexible units. The approximate degree of polymerization (number average) is 24.

MC2 is similar to MC1 except that the flexible spacers are much shorter and the degree of polymerization is only ~12.

The syntheses of SC1 and SC2,[4] as well as the monomeric chromophore[3] used as a dopant in DP, are described in other publications. We synthesized the main-chain polymers MC1 and MC2 by a convergent approach in which the donor (Scheme I) and acceptor (Scheme II) portions of the chromophores were constructed separately.[3] The two halves were joined by azo-coupling chemistry and were polymerized by conventional melt polycondensation in the presence of dibutyltin diacetate (Scheme III). The polymer in Scheme III with short spacer groups and side chain ($y = 1$; $z = 3$; R = Me) was crystalline ($T_m = 213$ °C) and exhibited poor solubility in prospective coating solvents, so thin films of this polymer could not be easily prepared. The other main-chain polymers (MC1 and MC2) were amorphous (by DSC and microscopy with

0024-9297/91/2224-4589$02.50/0

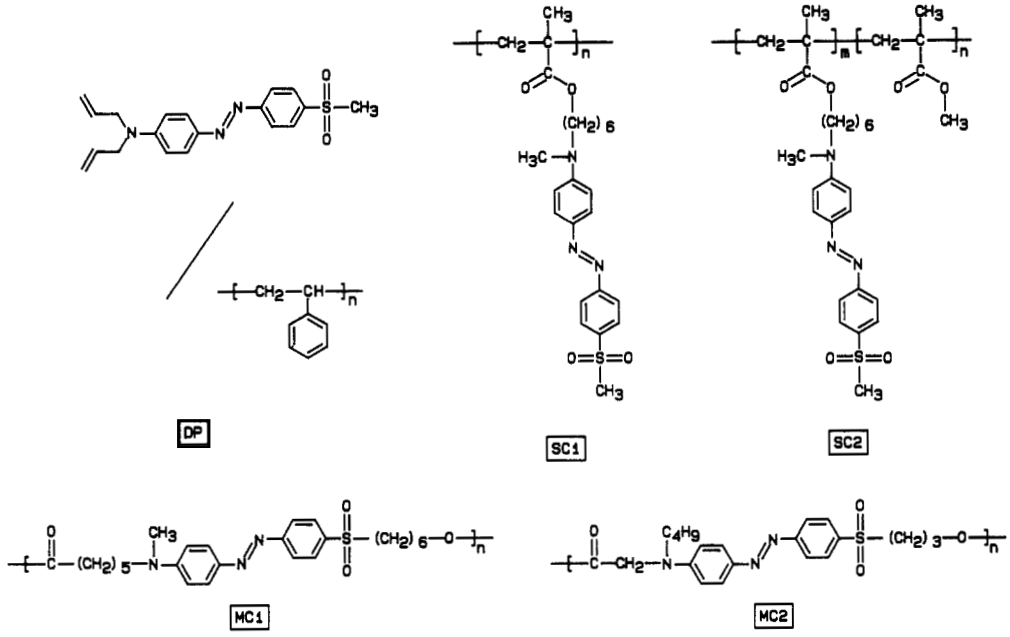

Figure 1. Chemical structures of the NLO polymers used in this study.

Scheme I
Synthesis of Donor Portion of Main-Chain NLO Polymers

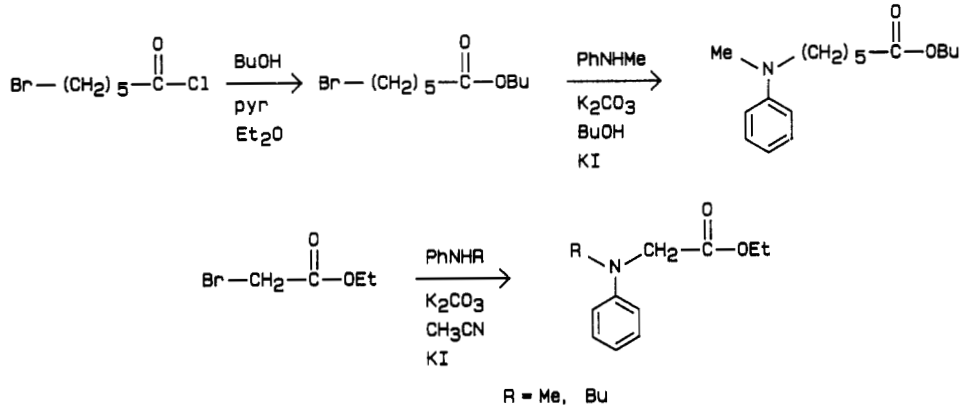

Scheme II
Synthesis of Acceptor Portion of Main-Chain NLO Polymers

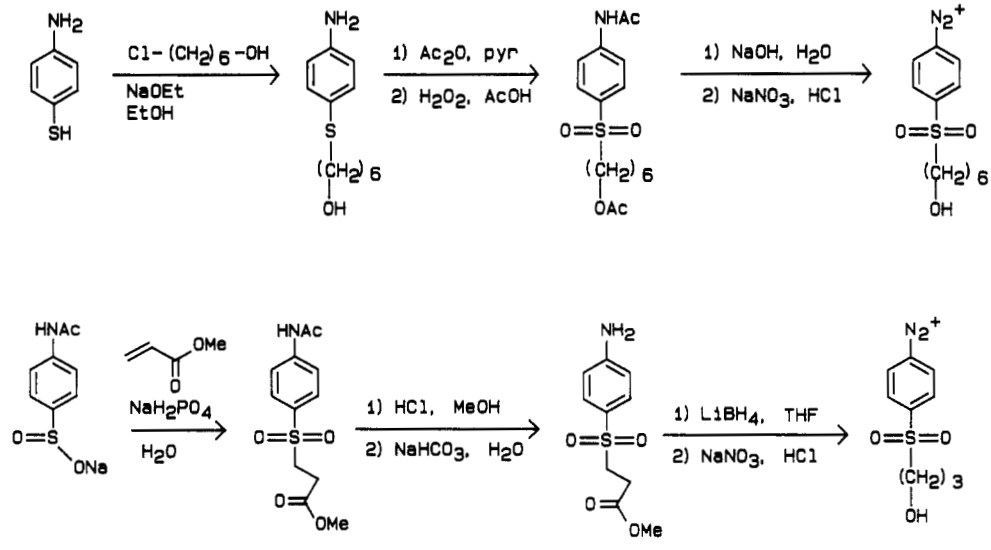

polarized light), and dissolved readily in chloroform, tetrahydrofuran, *N*,*N*-dimethylformamide, etc.

The molecular weight distributions of all of the soluble polymers were measured by size exclusion chromatography (SEC) using differential refractive index detection and monodisperse polystyrene standards, therefore the $\bar{M}_n$ and $\bar{M}_w$ values reported in Table I are only approximate. The absolute molecular weight distribution of MC1 was determined by SEC using viscometric detection and universal calibration, and its true $\bar{M}_n$ was found to be 12 000, as compared to the polystyrene equivalent $\bar{M}_n$ of 19 900. For copolymer SC2, SEC using absorbance

Scheme III
Synthesis of Main-Chain Polymers

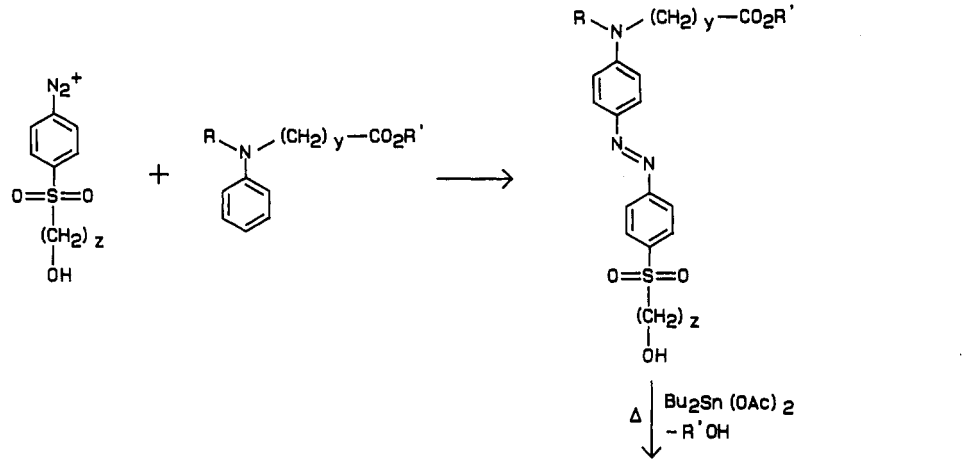

y	z	R	R'	
5	6	Me	Bu	(MC1)
1	3	Me	Et	
1	3	Bu	Et	(MC2)

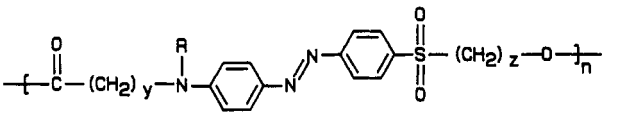

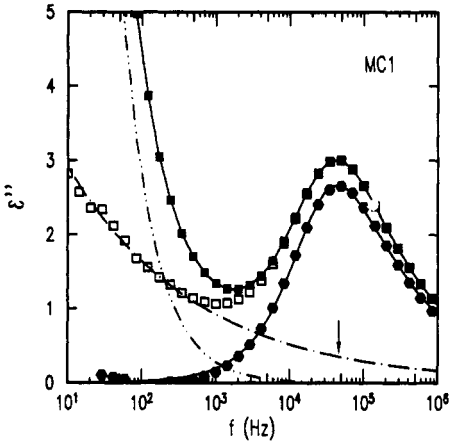

Figure 2. ϵ'' versus frequency for MC1 at 110 °C. Filled squares, raw data with dc conductivity background; open squares, low-frequency component $\propto f^{-0.25}$; filled hexagons, cleaned α relaxation peak with Havriliak–Negami fit.

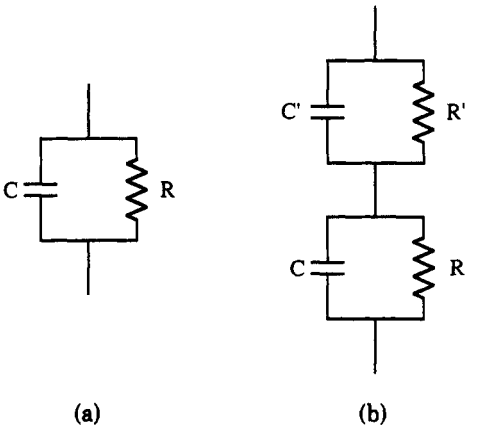

Figure 3. Equivalent circuits (a) without and (b) with interfacial polarization at the electrodes.

detection at 450 nm (the λ_{max} of the chromophore) gave results identical with the SEC run with differential refractive index detection, indicating that the chromophore-bearing repeat units were distributed uniformly in all molecular weight fractions.[4]

Samples for dielectric measurements were prepared by spin-coating the polymers from solution onto conductive substrates. After the samples were carefully dried, a conductive upper electrode was deposited on the film.

Data Analysis

General Procedure. In this section, the main characteristics observed in the experiments and the analysis of the data will be discussed. As a typical example, Figure 2 shows the imaginary part of the dielectric constant of MC1 at 110 °C as a function of frequency without any correction to the raw data (filled squares). The two prominent features, which can be found similarly in all polymers investigated, are a steep increase toward low frequencies, chiefly due to the dc conductivity, and a distinct absorption peak from the α relaxation of the dipoles associated with the NLO chromophores.

The sample forms a capacitor that may be viewed as an ideal loss free capacitor C in parallel to a resistor R, which accounts for the loss due to dipolar relaxation and for the dc conductivity of the polymer (Figure 3a). Formally, such a circuit can be described as a single capacitor with a complex dielectric constant $\epsilon^* = \epsilon' - i\epsilon''$, where

$$\epsilon' = C/C_0 \text{ and } \epsilon'' = (\omega RC_0)^{-1} \quad (1)$$

C_0 is the capacity if the polymer were replaced by vacuum[5] and $\omega = 2\pi f$, with f being the frequency in hertz.

In the absence of another loss mechanism, a constant dc conductivity $\sigma_{dc} = \epsilon_0/RC_0$ gives rise to a frequency dependence of ϵ'' that is proportional to $1/\omega$:

$$\epsilon_{dc}'' = \sigma_{dc}/\epsilon_0\omega \quad (2)$$

ϵ_0 is the permittivity of free space. In a plot of log ϵ'' versus log f, the dc conductivity regime shows up as a region with a slope of −1, as can be seen in Figure 4 at frequencies below the dipolar relaxation peak.

A number of different formulas have been used to describe the frequency dependence of the dielectric constant in the vicinity of dipolar absorption.[6,7] We will discuss our data in terms of the equation suggested by Havriliak and Negami,[8] which may be viewed as a superposition of individual Debye processes with a suitable

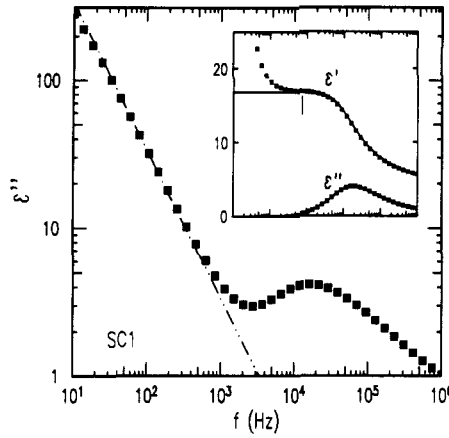

Figure 4. log–log plot of ϵ'' versus f for SC1 at 171 °C. The dc conductivity shows up as a straight line of slope −1. Inset: ϵ' and ϵ'' after dc conductivity background is removed. The solid lines are Havriliak–Negami functions determined by a fit to ϵ''. Note that the calculated curve for ϵ' contains no free parameters.

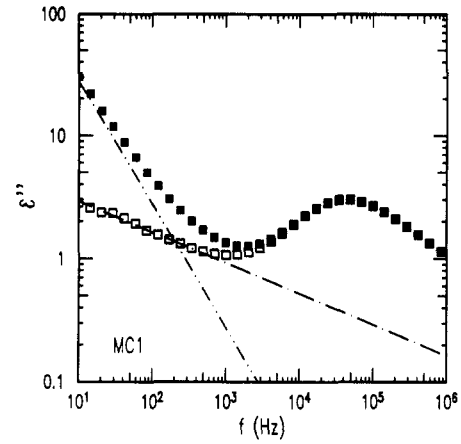

Figure 5. log–log plot of ϵ'' versus f for MC1 at 110 °C. The filled squares are the raw data. After the dc conductivity background (dashed line with slope −1) is removed, a straight line with slope −0.25 can be fitted to the low-frequency data.

distribution of relaxation times:[9]

$$\epsilon^* = \epsilon_u + (\epsilon_r - \epsilon_u)(1 + (i\omega\tau_o)^{1-\alpha})^{-\beta} \quad (3)$$

α and β are dimensionless parameters that determine the width and the shape of the relaxation time distribution function, and ϵ_u and ϵ_r are the unrelaxed and relaxed values of the dielectric constants. Equation 3 is a generalization of the formulas proposed by Cole and Cole ($\beta = 1$) and by Cole and Davidson ($\alpha = 0$). Separation of ϵ^* into real and imaginary parts results in rather lengthy expressions.[6]

Imaginary Part of the Dielectric Constant. Before the dipolar absorption peak in ϵ'' can be analyzed, the dc conductivity background must be determined. For the two side-chain polymers SC1 and SC2 and the doped polystyrene DP, this can easily be done by fitting a straight line with a slope of −1 to the low-frequency data as shown in Figure 4. After the background is subtracted, the imaginary part of the Havriliak–Negami function can be fitted to the loss peak (lower trace in the inset in Figure 4).

In the case of the two main-chain polymers, there is still a substantial deviation from the slope of −1, even far below the α peak (Figure 5). In these two cases, the low-frequency behavior of the generalized conductivity $\sigma = \epsilon''\epsilon_o\omega$ can be described by

$$\sigma = \sigma_{dc} + \sigma_\omega\omega^s \quad (4)$$

which is equivalent to

$$\epsilon'' = (\sigma_{dc}\omega^{-1} + \sigma_\omega\omega^{s-1})/\epsilon_o = \epsilon_{dc}'' + \epsilon_\omega'' \quad (5)$$

The open squares in Figures 2, 5, and 6 show what remains from the data after the dc contribution is removed. The second frequency-dependent part of eq 5 appears as a linear section in the log–log plot with a slope of $s - 1$. For the two main-chain polymers, the dimensionless parameter s is ~0.75 and, within the experimental error, independent of temperature. After this additional background contribution is subtracted, the corrected α relaxation peak is obtained, to which the Havriliak–Negami function can be fitted (Figures 2 and 6). There is some uncertainty in extending the power law found for ϵ_ω'' at lower frequencies toward the range of the α relaxation peak. This approach may be justified because power law behavior over many decades in frequency is typical for a wide variety of different dielectric loss mechanisms.[7]

Real Part of the Dielectric Constant. The real and imaginary parts of the dielectric constant are connected by the Kramers–Kronig relations.[6] The Havriliak–Negami function is expressed such that the relations are automatically obeyed. For $\epsilon_\omega'' = \sigma_\omega\omega^{s-1}/\epsilon_o$, the corresponding real part takes the form[10,11]

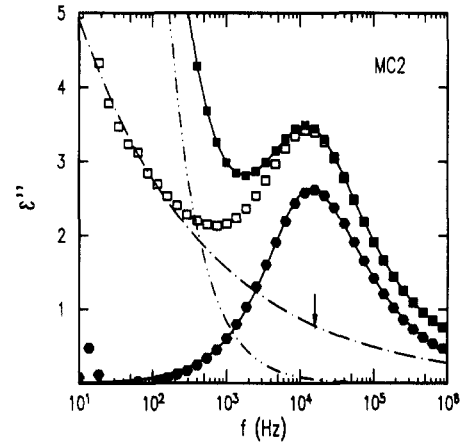

Figure 6. ϵ'' versus frequency for MC2 at 140 °C (see Figure 2).

$$\epsilon' = \tan\frac{s\pi}{2}\epsilon_\omega'' = \tan\frac{s\pi}{2}\sigma_\omega\omega^{s-1}/\epsilon_o \quad (6)$$

The Kramers–Kronig relations, however, do not apply to the loss due to the dc conductivity, and ϵ_{dc}'' has no correspondence in the real part of the dielectric constant.[6]

The insets in Figures 7 and 8 show the frequency dependence of ϵ', which was measured in the same experiment as was the ϵ'' data from Figures 2 and 6. The two dashed lines in the insets are the individual contributions to ϵ' as calculated from the Havriliak–Negami fit to the dipolar loss peak and from ϵ_ω'' by means of the Kramers–Kronig relations. Adding the two curves and shifting the result by ϵ_u, which is the unrelaxed dielectric constant as determined from room temperature measurements, gives the solid lines, which nearly perfectly reproduce the experimental data.

ϵ' and ϵ'' can be summarized in a Cole–Cole plot as in Figures 7 and 8, which show the traces for the raw data after subtraction of the dc background and the isolated α relaxation peaks as described by the Havriliak–Negami function (eq 3).

In case of the side-chain polymer SC1, there is no contribution from ϵ_ω'' and the real part of the dielectric constant is readily described by the transformation of the dipolar loss peak together with a shift by ϵ_u (upper trace in the inset in Figure 4), except for a deviation at the low-frequency side, which will be discussed in the next paragraph.

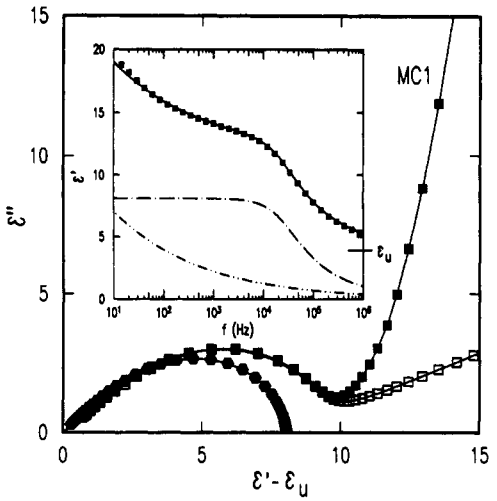

Figure 7. Cole–Cole plot for MC1 at 110 °C. Filled squares, raw data; open squares, after removing dc conductivity background; filled hexagons, α relaxation peak. Inset: ϵ' for MC1 at 110 °C. The solid line is calculated from ϵ'' without adjustable parameters.

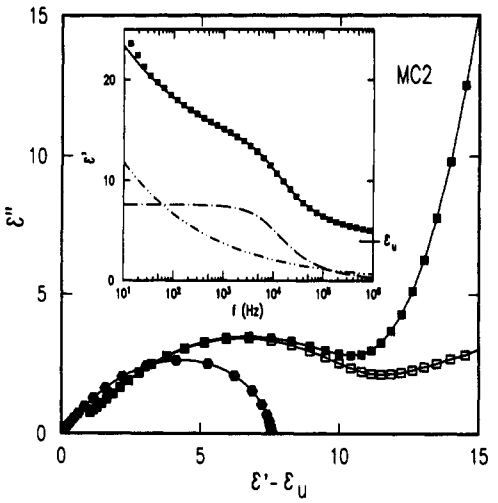

Figure 8. Cole–Cole plot and ϵ' for MC2 at 140 °C (see Figure 7).

Interfacial Polarization at the Electrodes. The steep increase of ϵ' at low frequencies in Figure 4 is correlated with a slight deviation of ϵ'' from the straight line in the log–log plot. This effect increases with temperature and is stronger in samples with a high dc conductivity. We attribute the effect to interfacial polarization (Maxwell–Wagner–Sillars effect) at partly blocking electrodes.[12] It is also observable in the main-chain polymers at higher temperatures and in the other side-chain polymer. In its simplest form, such interfacial polarization can be modeled by a resistor R' parallel to a capacitor C', which are both in series with the original sample (Figure 3b).

When ϵ^* is calculated from the experimental data, the sample is interpreted in terms of the circuit shown in Figure 3a, not the one in Figure 3b. Since the "wrong" circuit is used, an artificial frequency dependence of R and C is introduced, even in the absence of a frequency-dependent loss. The calculation of the resultant frequency dependence of ϵ^* is straightforward.[12] The interfacial polarization mimics an ideal Debye mechanism with an additional loss term from the dc conductivity:

$$\epsilon^* = \bar{\epsilon}_u + (\bar{\epsilon}_r - \bar{\epsilon}_u)(1 + (i\omega\bar{\tau}_o))^{-1} + i\bar{\sigma}/\omega \quad (7a)$$

$$\bar{\epsilon}_u = CC'/C_o(C + C') \quad (7b)$$

$$\bar{\epsilon}_r = (R^2C + R'^2C')/C_o(R + R')^2 \quad (7c)$$

$$\bar{\tau}_o = RR'(C + C')/(R + R') \quad (7d)$$

$$\bar{\sigma} = 1/C_o(R + R') \quad (7e)$$

Since the capacity C' of the polymer–electrode interface is much larger than the capacity C of the bulk polymer, the behavior at frequencies above $f = 1/2\pi\bar{\tau}_o$ approaches that of the circuit in Figure 3a. Thus R can be determined from the straight-line segment in Figure 4 and C from the plateau in ϵ' as marked in the inset. R' and C' are calculated by fitting eq 8 (see below) to the low-frequency part of ϵ' and ϵ''. Figure 9 shows the result of this procedure for SC1 at a relatively high temperature (180 °C), where the effect is more pronounced than at a lower one. The dashed lines correspond to what one would expect if the interfacial polarization were absent. The values for C and R are 862 pF and 383 kΩ, respectively, and the fit parameters are C' = 70 nF and R' = 275 kΩ, a result that is consistent with the initial assumption of $C' \gg C$.

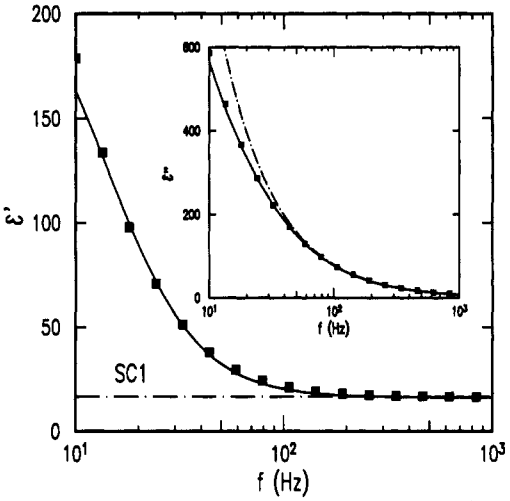

Figure 9. Effect of interfacial polarization at the electrode–polymer interface (SC1, 180 °C). The dashed lines show the behavior if the electrodes were completely nonblocking.

Results and Discussion

Thermal Stability. In general, the dipolar absorption peak could be reproduced very consistently for any given polymer and with very little variation between different samples. The low-frequency background, on the other hand, showed a much larger variability from sample to sample and increased for a given sample with the number of thermal cycles carried out. This effect is probably associated with thermal decomposition of the chromophores containing the weak azo linkage. Breaking this bond reduces the conjugation length of the π-electron system and causes a large blue shift in the optical absorption spectrum. To check this, a thin film of SC1 was spun onto a glass substrate and the absorption spectrum was recorded before and after the sample was subject to thermal treatment. There is a very slight loss of absorption noticeable after four temperature scans up to 170 °C at 1 °C/min and a pronounced one (20%) after the sample is stored at 170 °C overnight, indicating a substantial thermal decomposition of the chromophore in the latter case. At the same time, a strong increase of the low-frequency dielectric loss was observed.

dc Conductivity. The dc conductivities of representative samples of SC1, SC2, MC1, and MC2 were determined as described above, and their temperature dependences are summarized in Figure 10. Care must be taken in the extrapolation to zero frequency to take the apparent decrease of the bulk conductivity due to interfacial

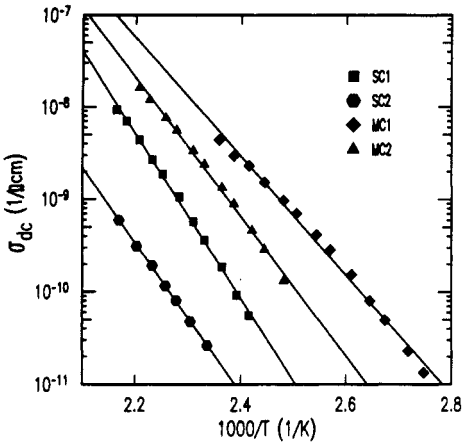

Figure 10. Arrhenius plot for dc conductivities. The activation energies are 168 (SC1), 153 (SC2), 121 (MC1), and 142 (MC2) kJ/mol.

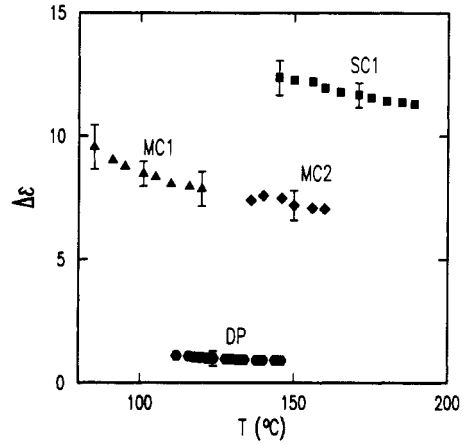

Figure 11. Relaxation strength of the α process as a function of temperature.

polarization at the electrodes into account. Apparent activation energies were determined by fitting Arrhenius functions to the data.

Dipolar α Relaxation. Except for the copolymer SC2, all samples studied showed only an α relaxation peak above the glass temperature T_g. These relaxations could be analyzed as described in the previous section. SC2 has an additional β relaxation (presumably due to the ester side groups in the copolymerized MMA units), which is very similar to the one observed in pure PMMA.[13] Since above T_g the α and β peaks overlap, it was not possible to separate the individual components. Therefore, the shape of the α peak was not analyzed for this polymer. All the other samples were analyzed as described above. The unrelaxed dielectric constants were measured at room temperature and are listed in the Table I. From the fit of the Havriliak–Negami function to the dipolar absorption peak, α, β, τ_0, and $\Delta\epsilon = \epsilon_r - \epsilon_u$ as defined in eq 3 are found. The $\Delta\epsilon$ values are plotted in Figure 11 as a function of temperature. Note that these values are not corrected for the thermal expansion of the polymer films. Within the experimental error, $\Delta\epsilon$ shows no temperature dependence that would exceed the usual $1/kT$ behavior.

After proper scaling, all loss peaks measured at different temperatures collapse onto a single master curve in the case of SC1 and the two main-chain polymers MC1 and MC2, indicating that the time–temperature superposition principle is obeyed and the distribution functions for the relaxation times do not change with temperature. The plot for MC1 is shown in Figure 12. The behavior for SC1 and MC2 is similar. The situation is different, however, for the doped polystyrene, in which a pronounced nar-

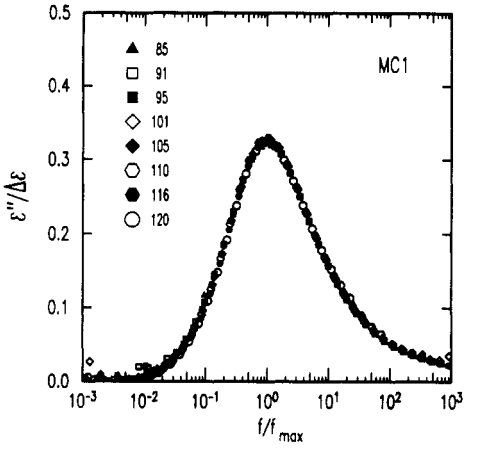

Figure 12. Master plot for normalized α peak of MC1.

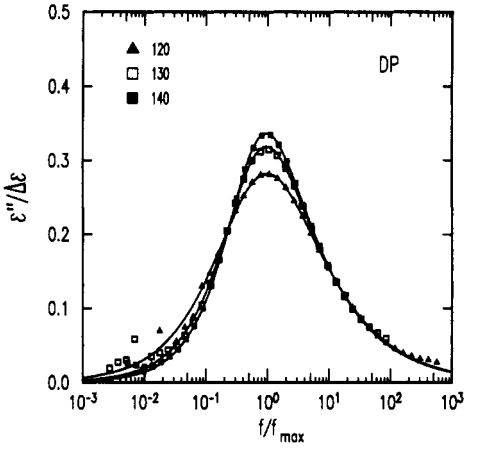

Figure 13. Normalized α peak of DP at different temperatures.

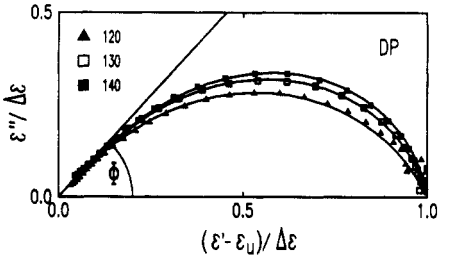

Figure 14. Cole–Cole plot for DP. The angle ϕ corresponds to $\beta(1 - \alpha) = 0.53$.

rowing of the loss peaks was observed as the temperature increased (Figure 13). This temperature dependence can also be seen in the Cole–Cole plots in Figure 14. The normalized Cole–Cole plots of the other polymers did not change with temperature.

Even though for the first three polymers (SC1, MC1, MC2) the loss peaks collapse neatly onto a common master plot if judged visually, the fit of the Havriliak–Negami function reveals a slight temperature dependence of the two parameters α and β. In Figure 15, the α, β data pairs for different temperatures are plotted for the four systems for which the loss peaks were analyzed. The solid lines are contour lines for a constant width (fwhm). The α, β values for SC1, MC1, and MC2 are approximately along this contour lines, indicating that the widths of their loss peaks do not change with temperature. The calculated Havriliak–Negami peaks that correspond to the two end points of the trace for a given polymer are nearly indistinguishable, if scaled so that the peak maxima coincide. Therefore, and because of the visual appearance of Figure 12, the temperature dependence of α and β has to be regarded as negligible within the experimental error and possibly as an artifact for these three polymers. The

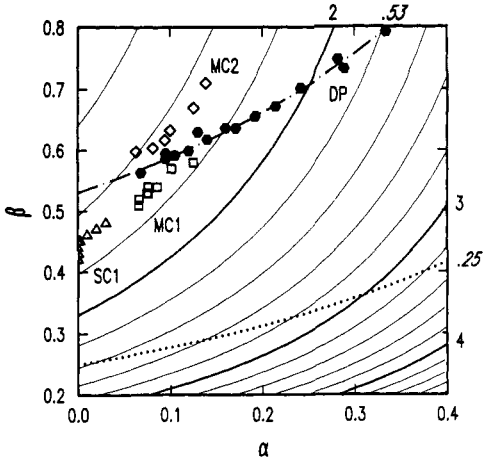

Figure 15. Plot of the a, β data pairs at different temperatures for various polymers. In all cases, the larger α values correspond to lower temperatures. The solid lines are contours for constant width of the Havriliak–Negami loss peak. The dashed lines correspond to the same asymptotic behavior at high frequencies. The slanted numbers give the product $\beta(1-\alpha)$.

problem is partly because the high-frequency wings are to some extent outside the accessible frequency window and that the low-frequency wings contain larger errors due to the dc conductivity background.

In the case of DP, the α, β values depend more strongly on temperature and do not evolve along a contour line but instead cross several, corresponding to a change in width from ca 2.22 decades in frequency at 116 °C to 1.65 at 146 °C. They lie, however, along another line, namely the one for $\beta(1-\alpha)$ = constant = 0.53 (dashed line in Figure 15). From the formulas for ϵ' and ϵ'' as given in ref 6, the asymptotic frequency dependence of ϵ^* is easily derived as

$$\lim_{\omega\to\infty}(\epsilon') = \epsilon_u + (\epsilon_r - \epsilon_u)\cos\{\beta \arctan[\cot(\pi\alpha/2)]\} \times (\omega\tau_0)^{-\beta(1-\alpha)} \quad (8a)$$

$$\lim_{\omega\to\infty}(\epsilon'') = (\epsilon_r - \epsilon_u)\sin\{\beta \arctan[\cot(\pi\alpha/2)]\}(\omega\tau_0)^{-\beta(1-\alpha)} \quad (8b)$$

Thus the high-frequency behavior of ϵ' and ϵ'' is governed by $\omega^{-\beta(1-\alpha)}$ and is therefore the same for all α, β pairs with $\beta(1-\alpha)$ = constant. While the shape and width of the loss peak in doped polystyrene changes with temperature, the form of its high-frequency wing remains invariant. This can also be seen from the constant angle[6] $\phi = \pi\beta(1-\alpha)/2$ under which the Cole–Cole plots for different temperatures intersect the ϵ' axis on the high-frequency side (Figure 14). The observed temperature dependence of the line width is reversible and does not change if the sample is driven through multiple temperature cycles. Thus the dependence cannot be attributed to permanent changes in the microenvironment of the dopant molecules.

The phenomenological Havriliak–Negami description was used to parameterize the data since it, or the somewhat less general Cole–Cole or Cole–Davidson formula, is the one most widely used in the literature to describe α relaxation processes in polymers. In the context of above observed temperature dependence, the model proposed by Jonscher[10,11] is very appealing. Jonscher discusses the dielectric response in terms of a many-body model where the motion of a dipole is coupled to two quite different time scales. The initial process is a fast jumplike reorientation of the dipoles that accounts for the high-frequency side of the loss peak. This sudden motion is followed by a much slower cooperative readjustment of the surrounding dielectric, which is responsible for the low-frequency wing.[10] Without ultimate proof, we assert that, within this framework, the temperature-independent shape of the high-frequency wing stems from the jumplike reorientation of the chromophores in their solvent cage. This process is associated with the dopant and thus extrinsic to the polymer. The temperature-dependent shape of the low-frequency side, on the other hand, reflects the polymer intrinsic dynamics of the readjusting chromophore environment.

At the present time we have no explanation of why this temperature dependence of the relaxation peak is absent if the chromophore is covalently attached to the polymer as in SC1, MC1, and MC2. This behavior is in contrast to that observed by Haines and Williams[21] for polystyrene doped with polar plasticizer. In that study, two distinct peaks were observed at concentrations ranging from those of the current study to a factor of 10 lower. This behavior was attributed to differences in the microenvironment of the plasticizer, probably due to aggregation effects.

Orientation of the End-to-End Vectors of the Main-Chain Polymers. In the Data Analysis section, the additional component ϵ_ω'' was described phenomenologically by a power law in frequency (eq 5), which contributes a substantial amount of relaxation strength for the two main-chain polymers at frequencies below the α relaxation. From least-squares fits, the parameter s was determined to be $s = 0.75 \pm 0.05$ for both MC1 and MC2. Within the accuracy of the experiment, s was independent of temperature.

Since both the high-frequency wing of the Havriliak–Negami loss peak and the ϵ_ω'' background can be described by such a power law, one can formally equate the two exponents from eq 5 and eq 8b and get $1 - s = \beta(1-\alpha)$ = constant (for a given polymer). The line that corresponds to $1 - s = 0.25$ is included in Figure 15 to allow comparison with the α relaxation peaks.

Power laws are found in a wide variety of dielectrics and are therefore termed by Jonscher the "universal dielectric response".[11] Sometimes a value of $s \cong 0.8$ is regarded as a proof for hopping conductivity as the underlying loss mechanism.[14] However, this is not the case in the two main-chain polymers MC1 and MC2. Here the global reorientation of the end-to-end vectors of the chains, or at least of larger segments, accounts for this low-frequency contribution to the loss. In the following paragraphs, a number of arguments will be presented to support this hypothesis.

The ground-state dipole moment of the NLO chromophore intersects the plane of the chromophore at an angle of ~35°.[15] Thus there is one component of the dipole perpendicular and one parallel to the chain contour. The perpendicular component can relax by local rotation around the long chromophore axis. In the case of the main-chain polymers, the parallel component of the dipole is coupled to the chain contour in a head-to-tail arrangement and thus to the end-to-end vector, which relaxes on a much slower time scale. The high-frequency tail of its relaxation peak appears as the additional low-frequency contribution observed in the main-chain polymers, but not in the side chain and the doped polymer. There the chromophores can completely orient by localized motions that are decoupled from the reorientation of the end-to-end vectors of the chains. Because the bulky chromophores need displacement of neighboring chains, their motions are coupled to the glass transition and show up in the α relaxation.

From Figure 11 one finds that the relaxation strength in the α peak of the main-chain polymers is only ~55% of the one in the side-chain polymer, even though the

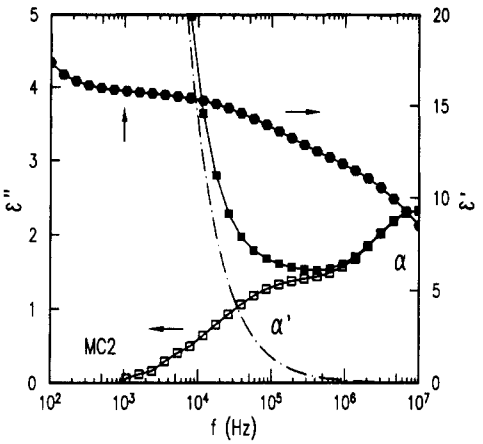

Figure 16. ϵ' and ϵ'' of MC2 in 1,2,3-trichloropropane (26.2% per weight) at 0 °C. The dashed line corresponds to the dc conductivity background of ϵ''.

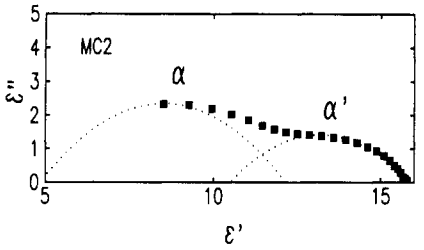

Figure 17. Cole–Cole plot for the data from Figure 16 after the conductivity background is removed. The dotted lines indicate the two underlying relaxation mechanisms.

number density of chromophores is roughly the same for SC1, MC1, and MC2. The contribution from the relaxation of the dipole moment component parallel to the chain is on the right order of magnitude to account for the difference. However, due to the limited frequency range of the experimental setup and because of the problems in removing the huge conductivity background at high temperatures and low frequencies, it was not possible to resolve the peak maximum and to obtain a precise number for the completely relaxed dielectric constant.

In optical frequency doubling and thermally stimulated discharge current experiments on the same main-chain polymers, we were able to distinguish clearly between the local rotation of the active chromophores and the global motion of the entire chains.[15] There the rotation around the long chromophore axis, which does not contribute significantly to second harmonic intensity, contributes ~37% to the polarization in MC2. The other 63% is attributed to the mode that produced the second harmonic. This situation is very close to what one would expect from the 35° angle between the dipole moment and the chain contour.[15] These numbers are compatible with the results of the dielectric experiments. Because of the flexibility provided by the long spacer units, there might also be some contribution to the α peak from the dipole moment parallel to the long chromophore axis due to localized librational modes around the short chromophore axes.

Experiments on Solutions. Another way of shifting the slow relaxation of the end-to-end vector toward higher and thus more accessible frequencies is to dissolve the polymer in a suitable solvent. In this case, the problem is one of getting the relaxation rates slow enough. To some extent this can be accomplished by increasing the viscosity of the solution by going to high concentrations and low temperatures. The results of such an experiment on MC2 in chloroform are summarized in Figures 16 and 17. After the dc conductivity background is removed, two loss peaks in ϵ'' can clearly be distinguished. The one at the higher frequency (α) is the one that corresponds to the α peak as observed in the polymer film. At lower frequencies the α' peak from the motion of the chain contour is clearly resolved. The slight increase of ϵ' around 100 Hz is due to electrode polarization as discussed in the context of the experiments on polymer films. Figure 17 shows the corresponding Cole–Cole plot. The unrelaxed dielectric constant must be slightly below that of the pure solvent (5.17 at 0 °C).

From measurements of the dielectric constant of dilute solutions as a function of concentration, the effective dipole moment per repeat unit was determined for SC1 and MC2 by a method proposed by Osipov.[16] Details of the experiment are described elsewhere.[15] If the fully relaxed dielectric constant is used, which can be found in Figure 16 at the plateau around 1 kHz, the values measured for SC1 and MC2 are 8.4 D (solvent 1,2,3-trichloropropane) and 8.2 D (solvent chloroform), respectively. These values are, within the experimental error, identical with the dipole moment of the dye monomer (8.3 D, solvent chloroform).[3] This result indicates that the spacer units provide enough flexibility to remove all orientational correlation between adjacent chromophores in the solution and the chains act like Gaussian chains, as far as the chromophores are concerned, equivalent to the vanishing of the sum in eq 9 (see below).

An attempt to correlate the dielectric constant of the polymer film with the dipole moment by means of the Kirkwood–Fröhlich formula[13] yield a correlation factor

$$g = 1 + \sum_{i \neq j} \langle \hat{\mu}_i \hat{\mu}_j \rangle \qquad (9)$$

which is only ~0.3 for SC1 and similar for the other polymers ($\hat{\mu}_k$ is the unit vector along the kth dipole moment). A correlation factor of less than unity means that, on average, the dipoles tend to favor an alignment in which components in opposite directions partly cancel each other. This result is in conflict with thermally stimulated discharge current experiments, which gave $g \cong 1.1$, and is discussed in more detail in ref 15. At the moment, the reason for this discrepancy is not known.

We can say, however, that no large-scale or extended dipolar correlation leading to enhanced alignment exists in these systems, contrary to what was reported previously for another main-chain system.[22] Even for the short spacer main-chain system, there seems to be sufficient flexibility in the linkage that the dipoles associated with the chromophores are largely uncorrelated.

Temperature–Frequency Shift. The frequency shift of the maximum of the α relaxation peak can be described by the Williams–Landel–Ferry (WLF) equation (Figure 18).

$$\log f = \frac{C_1(T - T_g)}{C_2 + T - T_g} + \log f_g \qquad (10)$$

f_g is the relaxation frequency at the glass temperature, and T_g and C_1 and C_2 are fit parameters. Within the free volume model, these parameters are related to the free volume fraction $f(T_g)$ and the free volume expansion coefficient $\alpha(T_g)$ at the glass temperature[13,17] by

$$f(T_g) = [C_1 \ln (10)]^{-1} \text{ and } \alpha(T_g) = f(T_g)/C_2 \qquad (11)$$

The results of the fit are summarized in Table I. The values found for $f(T_g)$ and $\alpha(T_g)$ are consistently somewhat larger than the "universal" values[13] of 0.025 and 4.8×10^{-4}, respectively. The experimental values are closest to the "universal" values for SC2, which is the polymer with the lowest chromophore concentration.

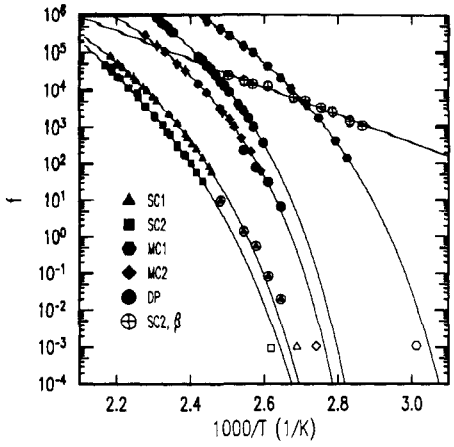

Figure 18. WLF fits to the frequency shift of the α relaxation. The open symbols are data from thermally stimulated discharge current experiments. The data on the straight line correspond to the β relaxation in SC2.

The open symbols in Figure 18 are the data points from thermally stimulated discharge current experiments that were done by heating the previously poled sample with a fixed rate q, thereby measuring the depolarization current released.[15] For a WLF temperature shift, an equivalent frequency f_{equ} for an ac experiment can be calculated by[18]

$$f_{equ} = \frac{1}{2\pi} q C_1 C_2 (C_2 + T_m - T_g)^{-2} \qquad (12)$$

T_m is the temperature of the maximum of the discharge current. The data points are very close to the extrapolated curves from the dielectric relaxation experiments, showing the self-consistency of the picture used to describe the temperature dependence of the relaxation rates.

For SC1 and MC2 rheological properties, G' and G'', were measured at temperatures of 105–120 °C. The a_T shift factors determined from the experiments are included in Figure 18 as encircled symbols. Note that the points are shifted by an arbitrary amount along the y axis. Their temperature dependence agrees well with the one found from the dielectric data.

The frequency shift of the β relaxation of the PMMA copolymer units in SC2 is also plotted in Figure 18. β relaxations are usually described by an Arrhenius law.[13] The activation energy as determined from the slope of the straight line fit is 72 kJ/mol, which is somewhat less than the 96 kJ/mol reported for pure PMMA.[19]

As pointed out earlier, the low-frequency component from the relaxation of the end-to-end vector in the two main-chain polymers cannot be resolved completely. Nevertheless, it is possible to get some estimation for its frequency shift factor. For both polymers it was found that the intensity at the frequency of the maximum of the α peak, as marked in Figures 2 and 6 with arrows, remains constant, even though the α peak shifts by several decades in frequency as the temperature is changed. Also the exponent s (eq 5) does not vary noticeably. Thus the time–temperature superposition principle seems to hold for both relaxation modes with the same shift factor.

The larger background from the overall chain reorientation (global mode) at the frequency of the α peak in the case of MC2 reflects a relatively faster mean relaxation rate for the reorientation of the main chains as compared to MC1. This difference may be caused by the difference in the average chain lengths of both polymers. Note however, that the shape of the high-frequency wing of the global mode, which is determined by the exponent s in eq 5, is very similar for MC1 and MC2 and does not depend on the degree of polymerization. Apparently it reflects the *short-range* connectivity of the dipoles in the chain.

Experimental Section

Materials. NMR spectra were obtained on a General Electric QE-300 instrument operating at 300 MHz for ^{1}H and 75.5 MHz for ^{13}C. Chemical shifts are reported in parts per million downfield from internal trimethylsilane. All NMR coupling constants are reported in hertz. Mass spectra were obtained by field desorption (FD-MS). Approximate molecular weight distributions were determined by size exclusion chromatography (SEC) using polystyrene standards and differential refractive index detection. Absolute molecular weights were measured by SEC using viscometric detection and universal calibration. Elemental analyses were performed by Eastman Kodak Co., Analytical Technologies Division.

Butyl 6-Bromohexanoate. To a stirred mixture of butanol (39 g, 0.52 mol), 42 g (0.52 mol) of pyridine, and 550 mL of anhydrous ether was added dropwise 6-bromohexanoyl chloride (100 g, 0.47 mol). The reaction mixture was stirred at 23 °C for 1 h and then filtered. The filtrate was washed with equal volume portions of water, 5% $NaHCO_3$, and again water. The organic layer was dried over $MgSO_4$, and the solvent was removed. The resulting oil was distilled at reduced pressure, bp 120–125 °C (0.1 mm), to produce 111 g (94%) of a colorless oil.

***N*-[(5-Butoxycarbonyl)pentyl]-*N*-methylaniline.** A mixture of 111 g (0.44 mol) of butyl 6-bromohexanoate, 50 g (0.46 mol) of *N*-methylaniline, 63.9 g of potassium carbonate, 3.65 g of potassium iodide, and 500 mL of butanol was heated at reflux with vigorous stirring under nitrogen for 60 h. The reaction mixture was filtered and the filtrate was concentrated. The residue was dissolved in ethyl acetate and washed with water. The organic layer was dried over $MgSO_4$, and the solvent was evaporated. The resulting oil was distilled at reduced pressure (0.1 mm) to produce 60 g (50%) of a yellow oil: bp 183–188 °C; ^{1}H NMR ($CDCl_3$) δ 0.95 (t, J = 7.3, 3 H), 1.4 (m, 4 H), 1.6 (m, 6 H), 2.32 (t, J = 7.4, 2 H), 2.93 (s, 3 H), 3.31 (t, J = 7.5, 2 H), 4.08 (t, J = 6.6, 2 H), 6.71 (m, 3 H), 7.24 (m, 2H); IR (neat) 2940, 1735, 1598, 1504, 1160, 745, 739 cm^{-1}.

Ethyl *N*-Methyl-*N*-phenylglycinate. A mixture of *N*-methylaniline (198 g, 1.85 mol), ethyl chloroacetate (227 g, 1.85 mol), potassium carbonate (256 g, 1.85 mol), potassium iodide (15 g, 0.93 mol), and 750 mL of absolute ethanol was stirred at reflux for 72 h, then cooled, and filtered. The solvent was removed from the filtrate at reduced pressure, and the residue was fractionally distilled in vacuo. A slightly yellow oil was obtained: yield 162 g (45%); ^{1}H NMR ($CDCl_3$) δ 1.24 (t, J = 7.1, 3 H), 3.07 (s, 3 H), 4.06 (s, 2 H), 4.17 (q, J = 7.1, 2 H), 6.75 (m, 3 H), 7.20 (m, 2 H); IR (neat) 1748, 1602, 1507, 1191 cm^{-1}.

Ethyl *N*-Butyl-*N*-phenylglycinate. The above procedure was repeated starting with 99.0 g (0.663 mol) of *N*-butylaniline, 115 g (0.689 mol) of ethyl bromoacetate, 93.0 g (0.673 mol) of potassium carbonate, 6.0 g (0.036 mol) of potassium iodide, and 400 mL of acetonitrile (solvent). The crude product was fractionally distilled at reduced pressure, and 126 g (81%) of a gold oil was collected: bp 130–135 °C (0.065 mm); ^{1}H NMR (300 MHz, $CDCl_3$) δ 0.95 (t, J = 7.2, 3 H), 1.24 (t, J = 7.1, 3 H), 1.35 (m, 2 H), 1.60 (m, 2 H), 3.36 (t, J = 7.6, 2 H), 4.00 (s, 2 H), 4.17 (q, J = 7.2, 2 H), 6.61 (d, J = 8.4, 2 H), 6.69 (t, J = 7.2, 1 H), 7.19 (t, J = 7.9, 2 H); FD-MS m/e 235 (M^+).

4-Aminophenyl 6-Hydroxyhexyl Sulfide. Sodium metal (24 g, 1.0 mol) was dissolved in 200 mL of absolute ethanol with stirring under nitrogen. 4-Aminothiophenol (125 g, 1.0 mol) was added in small portions; then 6-chlorohexanol (143 g 1.0 mol) was added. The resulting mixture was heated at reflux for 1 h and filtered, and the filtrate was concentrated. The residue was dissolved in dichloromethane, and the solution was washed with water, 5% $NaHCO_3$, and again with water. The organic layer was dried (Na_2SO_4), the solvent was evaporated, and the residue was recrystallized from chloroform/heptane to yield 156 g (70%) of slightly yellow crystals.

4-Acetamidophenyl 6-Acetoxyhexyl Sulfide. A solution comprising 155 g (0.7 mol) of 4-aminophenyl 6-hydroxyhexyl sulfide, 175 g (1.75 mol) of acetic anhydride, and 140 g (1.75 mol) of pyridine was heated at reflux with stirring for 2 h. The solution was poured onto ice, and the precipitated product was collected by filtration and washed with water, 5% HCl, and again with

water. The product was recrystallized from methanol/water to produce 155 g (71%) of a slightly yellow solid: ^{1}H NMR ($CDCl_3$) δ 1.40 (m, 4 H), 1.62 (m, 4 H), 2.04 (s, 3 H), 2.17 (s, 3 H), 2.86 (t, J = 7.3, 2 H), 4.04 (t, J = 6.7, 2 H), 7.3 (overlapping s and d, 3 H), 7.42 (d, J = 8.6, 2 H).

4-Aminophenyl 6-Hydroxyhexyl Sulfone. A mixture of 145 g (0.47 mol) of 4-acetamidophenyl 6-acetoxyhexyl sulfide and 600 mL of glacial acetic acid was heated to reflux with stirring. Hydrogen peroxide (140 g, 30% solution) was added in small portions, and the resulting mixture was stirred at reflux for 3 h. The reaction mixture was concentrated, and the residue was dissolved in dichloromethane. The solution was washed with water and dried ($MgSO_4$), and the solvent was evaporated to deposit a tan oil. The oil was heated at reflux with stirring for 16 h in 500 mL of 50% aqueous ethanol containing 10% NaOH. The resulting solution was extracted with ether, the extract was dried ($MgSO_4$), and the solvent was removed. The residue was recrystallized from ethanol/water to produce 74 g (65%) of slightly yellow crystals: ^{1}H NMR ($(CD_3)_2SO$) δ 1.2 (m, 6 H), 1.45 (m, 2 H), 3.03 (t, J = 7.8, 2 H), 3.30 (m, 2 H), 4.28 (t, J = 5.2, 1 H), 6.08 (s, 2 H), 6.60 (d, J = 8.6, 2 H), 7.42 (d, J = 8.6, 2 H).

Ethyl 3-[(4-Acetamidophenyl)sulfonyl]propionate. A solution of sodium 4-acetamidobenzenesulfinate (200 g, 1.0 mol) and sodium dihydrogen phosphate hydrate (139 g, 1.0 mol) in 1000 mL of water was stirred mechanically at 23 °C, and a solution of ethyl acrylate in 100 mL of tetrahydrofuran (THF) was added. The reaction mixture was stirred at 23 °C for 72 h, and the resulting white solid was filtered, washed with water, and air-dried. The product was recrystallized from 2-butanone and dried in vacuo: yield 243 g (81%); mp 125–128 °C (lit.[20] mp 128–129 °C).

Ethyl 3-[(4-Aminophenyl)sulfonyl]propionate. A mixture of 173 g (0.578 mol) of ethyl 3-[(4-acetimidophenyl)sulfonyl]propionate, 630 mL of absolute ethanol, and 70 mL of concentrated HCl was heated at reflux for 16 h and then cooled. The white crystals of the amine hydrochloride that formed on standing were collected and washed with cold ethanol and with ether. The free amine was liberated by suspending the solid in 1600 mL of saturated aqueous sodium bicarbonate. (CAUTION: Foaming.) The product was collected, washed with water, and dried in vacuo: yield 110 g (74%); ^{1}H NMR ($(CD_3)_2SO$) δ 1.16 (t, J = 7.1, 3 H), 2.56 (t, overlapping with solvent peak, 2 H), 3.36 (t, 2 H), 3.99 (t, J = 7.1, 2 H), 6.20 (s, 2 H), 6.66 (d, J = 8.6, 2 H), 7.46 (d, J = 8.6, 2 H).

4-[3-Hydroxypropyl)sulfonyl]aniline. Ethyl 3-[(4-aminophenyl)sulfonyl]propionate (109 g, 0.424 mol) was dissolved in 500 mL of dry THF and heated to reflux under nitrogen with mechanical stirring. A 2.0 M solution of lithium borohydride in THF (260 mL) was added dropwise to the solution at reflux, after which time the mixture was held at reflux for 4 h. A thick white precipitate formed on cooling to 23 °C. Aqueous 10% HCl was added carefully (CAUTION: vigorous foaming) to decompose excess hydride and then the mixture was neutralized by the addition of 5% aqueous $NaHCO_3$. The aqueous layer of the resulting two-phase mixture was saturated with NaCl, and the organic layer was dried ($MgSO_4$) and concentrated. A tan solid deposited, and after recrystallization from 95% methanol/5% ether and drying in vacuo, 58.8 g (60%) of white solid was obtained: mp 104.5–106.5 °C; ^{1}H NMR ($(CD_3)_2SO$) δ 1.6 (m, 2 H), 3.08 (t, J = 7.8, 2 H), 3.37 (m, 2 H), 4.56 (t, J = 5.4, 1 H), 6.09 (s, 2 H), 6.64 (d, J = 8.7, 2 H), 7.44 (d, J = 8.7, 2 H).

4-[[5-(Butoxycarbonyl)pentyl]methylamino]-4′-[(6-hydroxyhexyl)sulfonyl]azobenzene. A stirred suspension of 7.2 g (28 mmol) of 4-aminophenyl 6-hydroxyhexyl sulfone in 60 mL of 10% aqueous HCl was cooled to 0–5 °C and treated dropwise with 2.1 g (31 mmol) of sodium nitrite dissolved in 10 mL of water. The sulfone dissolved. After 15 min of stirring, 7.8 g (28 mmol) of N-[5-(butoxycarbonyl)pentyl]-N-methylaniline was added, and the reaction mixture was gradually warmed to 23 °C and stirred for 16 h. The precipitated product was extracted with dichloromethane, the extract was washed with water and dried ($MgSO_4$), and the solvent was removed to deposit an orange solid. The product was recrystallized from toluene and then from 50% hexanes/tetrahydrofuran to yield 8.1 g (53%) of an orange powder: ^{1}H NMR ($CDCl_3$) δ 0.93 (t, J = 7.3, 3 H), 1.3–1.8 (m, 19 H), 2.32 (t, J = 7.4, 2 H), 3.08 (s, 3 H), 3.11 (t, J = 9.1, 2 H), 3.44 (t, J = 7.4, 2 H), 3.60 (t, J = 6.4, 2 H), 4.07 (t, J = 6.6, 2 H), 6.72 (d, J = 9.1, 2 H), 7.88 (d, J = 9.1, 2 H), 7.96 (AB, $\Delta\nu$ = 9.3, J = 8.8, 4 H); ^{13}C{^{1}H} NMR ($CDCl_3$) δ 13.7, 19.2, 22.7, 24.8, 25.2, 26.6, 26.8, 28.1, 30.7, 32.3, 34.2, 38.7, 52.5, 56.4, 62.6, 64.3, 111.3, 122.7, 126.0, 129.1, 138.4, 143.5, 152.3, 156.5, 173.6.

4-[[(Ethoxycarbonyl)methyl]methylamino]-4′-[(3-hydroxypropyl)sulfonyl]azobenzene. The above procedure was repeated using 11.0 g (56.9 mmol) of ethyl N-methyl-N-phenylglycinate, 10.2 g (47.4 mmol) of 4-[(3-hydroxypropyl)sulfonyl]-aniline, and 4.4 g (64 mmol) of sodium nitrite. The product was recrystallized from toluene and dried in vacuo: yield 12.1 g (61%) of orange powder; mp 129.5–131 °C; ^{1}H NMR ($CDCl_3$) δ 1.27 (t, J = 7.1, 3 H), 1.82 (br s, 1 H), 2.00 (m, 2 H), 3.20 (s, 3 H), 3.28 (t, J = 7.6, 2 H), 3.74 (t, J = 5.9, 2 H), 4.18 (s, 2 H), 4.23 (q, J = 7.1, 2 H), 6.75 (d, J = 9.1, 2 H), 7.90 (d, J = 9.1, 2 H), 8.00 (AB, $\Delta\nu$ = 12.0, J = 8.7, 4 H); ^{13}C{^{1}H} NMR ($CDCl_3$) δ 14.2, 25.8, 39.9, 53.4, 54.3, 60.5, 61.4, 111.8, 122.8, 123.8, 129.1, 138.5, 144.3, 152.2, 156.2, 170.0; FD-MS m/e 419 (M^+). Anal. Calcd for $C_{20}H_{25}N_3O_5S$: C, 57.26; H, 6.01; N, 10.02; S, 7.64. Found: C, 57.34; H, 5.75; N, 9.96; S, 7.55.

4-[[(Ethoxycarbonyl)methyl]butylamino]-4′-[(3-hydroxypropyl)sulfonyl]azobenzene. The above procedure was repeated using 25.0 g (0.116 mol) of 4-[(3-hydroxypropyl)sulfonyl]-aniline, 8.81 g (0.128 mol) of sodium nitrite, and 30.1 g (0.128 mol) of ethyl N-butyl-N-phenylglycinate. The product was recrystallized from toluene/heptane and then from absolute ethanol and dried in vacuo: yield 36.1 g (69%) of orange powder; mp 75–77 °C; ^{1}H NMR ($CDCl_3$) δ 0.98 (t, J = 7.3, 3 H), 1.27 (t, J = 7.1, 3 H), 1.40 (m, 2 H), 1.68 (m, 2 H), 1.97 (m, 2 H), 2.13 (br s, 1 H), 3.26 (t, J = 7.6, 2 H), 3.48 (t, J = 7.6, 2 H), 3.69 (t, J = 5.9, 2 H), 4.13 (s, 2 H), 4.22 (q, J = 7.1, 2 H), 6.69 (d, J = 9.1, 2 H), 7.88 (d, J = 9.1, 2 H), 7.96 (AB, $\Delta\nu$ = 11.6, J = 8.7, 4 H); ^{13}C{^{1}H} NMR ($CDCl_3$) δ 13.9, 14.1, 20.1, 25.7, 29.4, 52.2, 52.7, 53.4, 60.3, 61.3, 111.5, 122.7, 125.8, 129.0, 138.3, 144.0, 151.4, 156.2, 170.1; FD-MS m/e 461 (M^+). Anal. Calcd for $C_{23}H_{31}N_3O_5S$: C, 59.85; H, 6.77; N, 9.10; S, 6.95. Found: C, 59.50; H, 6.75; N, 8.93; S, 7.17.

Polymerization of 4-[[5-(Butoxycarbonyl)pentyl]methylamino]-4′-[(6-hydroxyhexyl)sulfonyl]azobenzene. 4-[[5-(Butoxycarbonyl)pentyl]methylamino]-4′-[(6-hydroxyhexyl)-sulfonyl]azobenzene (4.8 g, 8.8 mmol) was placed in a side-arm flask, evacuated to 10^{-3} mm, and heated with stirring at 155 °C for 5 h. The material was cooled, and four drops of dibutyltin diacetate was added. The compound was remelted under vacuum with stirring and heated at 155 °C for 16 h and at 175 °C for 5 h. The product was cooled, dissolved in dichloromethane, and precipitated into excess methanol. The resulting solid was filtered, air-dried, and reprecipitated from dichloromethane into methanol. After drying at 100 °C in vacuo, a tough red solid was obtained: mass 3.8 g (91%); ^{1}H NMR ($CDCl_3$, all peaks were broad) δ 1.4 (m, 6 H), 1.7 (m, 8 H), 2.31 (t, J = 7.2, 2 H), 3.07 (s, 3 H), 3.10 (t, $J \cong 8$, 2 H), 3.43 (t, J = 7.0, 2 H), 4.03 (t, J = 6.3, 2 H), 6.72 (d, J = 8.9, 2 H), 7.88 (d, J = 8.8, 2 H), 7.97 (AB, $\Delta\nu$ = 6.8, J = 8.9, 4 H). End group signals at δ 0.93 and 3.6 were barely detectable above base-line noise; ^{13}C{^{1}H} NMR ($CDCl_3$) δ 22.6, 25.5, 26.5, 26.8, 27.9, 28.3, 34.1, 38.7, 52.4, 56.3, 64.1, 111.3, 122.7, 126.3, 129.0, 138.2, 143.4, 152.3, 156.4, 173.5. T_g at 59 °C. Polystyrene equivalent $\overline{M}_n$ 19 900; $\overline{M}_w$ 70 600. Absolute $\overline{M}_n$ 12 000; $\overline{M}_w$ 39 400.

Polymerization of 4-[[(Ethoxycarbonyl)methyl]methylamino]-4′-[(3-hydroxypropyl)sulfonyl]azobenzene. The above procedure was repeated using 4.6 g of 4-[[(ethoxycarbonyl)-methyl]methylamino]-4′-[(3-hydroxypropyl)sulfonyl]azobenzene. The product was only soluble in hot N,N-dimethylformamide, but precipitated on cooling. T_g at 113 °C; T_m at 213 °C (onset).

Polymerization of 4-[[(Ethoxycarbonyl)methyl]butylamino]-4′-[(3-hydroxypropyl)sulfonyl]azobenzene. A molten sample of 4-[[(ethoxycarbonyl)methyl]butylamino]-4′-[(3-hydroxypropyl)sulfonyl]azobenzene (17.6 g) plus five drops of dibutyltin diacetate was heated for 15 h with stirring under vacuum 4×10^{-3} mm at 155 °C. The product was cooled, dissolved in dichloromethane, and precipitated into excess methanol. The polymer was reprecipitated from dichloromethane into methanol and then from THF into deionized water. After filtration and drying in vacuo, 15.0 g (94%) of orange powder was obtained: ^{1}H NMR ($CDCl_3$, all peaks were broad) δ 0.96 (t, J = 7.2, 3 H), 1.4 (m, 2 H), 1.6 (m, 2 H), 2.1 (m, 2 H), 3.1 (t, 2 H), 3.4 (t, 2 H),

4.13 (s, 2 H), 4.2 (t, 2 H), 6.65 (d, J = 8.9, 2 H), 7.82 (d, J = 8.8, 2 H), 7.9 (m, 4 H). Integration of the residual end group signal at δ 3.3 suggested a degree of polymerization, $\overline{X}_n$, of 8; $^{13}C\{^1H\}$ NMR ($CDCl_3$) δ 13.9, 20.1, 22.3, 29.5, 52.2, 52.7, 53.0, 62.9, 111.5, 122.9, 125.9, 129.0, 138.1, 144.0, 151.3, 156.2, 169.9. T_g at 92 °C. Polystyrene equivalent $\overline{M}_n$ 4900; $\overline{M}_w$ 11 500. Anal. Calcd for $C_{21}H_{25}N_3O_4S$: C, 60.70; H, 6.06; N, 10.11; S, 7.72. Found: C, 59.35; H, 6.12; N, 9.58; S, 8.13.

Polymer Thin-Film Samples and Dielectric Measurements. The samples were prepared by spin-coating polymer films of 1.5–2-μm thickness onto a glass substrate covered with a thin gold electrode. After the solvent was removed by baking the samples in a vacuum oven at or above the T_g of the polymers for several hours, a second electrode was evaporated on top of the polymer film. The sample make-up is in detail in ref 15, with the only difference that for the optical experiments discussed herein one gold electrode was replaced by indium tin oxide. An environmental chamber (9023, Delta Design) was used to control the sample temperature. The complex impedance was measured as a function of frequency at typically 50–100 different temperatures with a HP4192A impedance analyzer (5 Hz–13 MHz, Hewlett-Packard). The oscillator voltage was 1 V peak to peak (pp). No change in the data was seen at a lower oscillator voltage of 0.1 V (pp) and at a higher voltage of up to 30 V (pp). The latter measurement was done with less sensitivity by using a sine wave generator and an oscilloscope to measure current and phase shift. Data acquisition and evaluation was done with a computer. For the measurements on solutions a gold-plated liquid cell (DFL2, Kahlsico) was used.

The absolute values obtained for the dielectric constants contain an error of ~5%, which stems mainly from the difficulty of determining the geometrical dimensions of the sample capacitor, especially its thickness, precisely.

Conclusions

The dielectric behavior of a series of five different polymers containing the same nonlinear optical chromophore (as a dopant, or tethered to a side chain or within the main chain) has been studied and compared. In all cases the relaxation of the chromophores is coupled to the glass transition, which indicates an α process whose temperature shift can be described by the WLF equation with C_1 and C_2 close to the "universal" values. Results from thermally stimulated discharge current and mechanical rheological experiments agree well with the dielectric data.

The host–guest system shows a narrowing of the rate distribution function with increasing temperature that affects primarily the low-frequency side of the relaxation peak. For the polymers with covalently attached chromophores, the time–temperature superposition principle holds.

In the two main-chain polymers, an additional slow relaxation mode at frequencies below the α peaks was found. This mode is consistent with the global reorientation of the end-to-end vectors of the chains. Future experiments will address the molecular weight dependence of the individual relaxations, because the chain length should exert only a minor influence on the local relaxation modes but cause a major change on the global modes of the main chain polymers.

Acknowledgment. We thank M. Scozzafava and P. T. Dao for their help with the sample preparation, J. J. Fitzgerald for use of his dielectric relaxation equipment, J. M. O'Reilly for measuring rheological properties of the polymers, for many helpful discussions, and for carefully reading the manuscript, J. Phelan for measuring refractive indices, A. Friedrich (Colgate University intern) for synthetic assistance, A. Ulman and T. E. Long for providing the dye and the polystyrene used in one of the samples, all members of Eastman Kodak Co. Research Laboratories. We also thank the following members of Kodak Analytical Technology Division: M. Moscato and V. Mazzio for thermal measurements, T. Criswell for mass spectra, and M. Thomas, S. Miller, and T. Mourey for size exclusion measurements.

References and Notes

(1) Williams, D. J. In *Nonlinear Optical Properties of Organic Molecules and Crystals*; Chemla, D. S., Zyss, J., Eds.; Academic Press: New York, 1987.
(2) Williams D. J. In *Electronic and Photonic Applications of Polymers*, ACS Advances in Chemistry 218; Bowden, M. J., Turner, S. R., Eds.; American Chemical Society: Washington, DC, 1988.
(3) Ulman, A.; Willand, C. S.; Köhler, W.; Robello, D. R.; Williams, D. J.; Handley, L. *J. Am. Chem. Soc.* **1990**, *112*, 7083.
(4) Robello, D. R.; Schildkraut, J. S.; Dao, P.; Scozzafava, M.; Ulman, A.; Willand, C. S., submitted for publication.
(5) Eich, M.; Sen, A.; Looser, H.; Bjorklund, G. C.; Swalen, J. D.; Twieg, R.; Yoon, D. Y. *J. Appl. Phys.* **1989**, *66*, 2559.
(6) Böttcher, C. J. F.; VanBelle, O. C.; Bordewijk, P. *Theory of Electric Polarization*, 2nd ed.; Elsevier: New York, 1978.
(7) Jonscher, A. K. *Nature* **1977**, *267*, 673.
(8) Havriliak, S., Jr.; Negami, S. *J. Polym. Sci., Part C* **1966**, *14*, 99.
(9) Havriliak, S., Jr.; Negami, S. *Polymer* **1967**, *8*, 161.
(10) Jonscher, A. K. *J. Mater. Sci.* **1981**, *16*, 2037.
(11) Jonscher, A. K. *Nature* **1974**, *250*, 191.
(12) Pochan, J. M.; Pai, D. M. In *Plastics Polymer Science and Technology*; Baijal, M. D., Ed.; Wiley-Interscience: New York, 1982.
(13) McCrum, N. G.; Read, B. E.; Williams, G. *Anelastic and Dielectric Effects in Polymeric Solids*; Wiley: New York, 1967.
(14) Kremer, F.; Vallerien, S. U.; Zentel, R.; Kapiza, H. *Macromolecules* **1989**, *22*, 4040.
(15) Köhler, W.; Robello, D. R.; Dao, P. T.; Willand, C. S.; Williams, D. J. *J. Chem. Phys.* **1990**, *93*, 9157.
(16) Osipov, O. A.; Panina, M. A.; *Zh. Fiz. Khim.* **1958**, *32*, 2287.
(17) Bailey, T. T.; North, A. M.; Pethrick, R. A. *Molecular Motions in High Polymers*; Claerndon Press: Oxford, U.K., 1981.
(18) Vanderschueren, J.; Gasiot, J. *Topics in Applied Physics: Thermally Stimulated Relaxations in Solids*; Braunlich, P., Ed.; Springer: Berlin, 1979; Vol. 37.
(19) Brouckere, L.; Offergeld, G. *J. Polym. Sci.* **1958**, *30*, 105.
(20) Achmatowicz, O.; Michalski, *J. Rocz. Chem.* **1965**, *30*, 243; *Chem. Abstr.* **1961**, *54*, 1064b.
(21) Hains, P. J.; Williams, G. *Polymer* **1975**, *16*, 725.
(22) Willand, C. S.; Williams, D. J. *Ber. Bunsenges. Phys. Chem.* **1987**, *53*, 5538.

Registry No. DP, 9003-53-6; SC1 (homopolymer), 131825-90-6; SC2 (copolymer), 133418-82-3; MC1, 130805-82-2; MC1 (homopolymer), 130805-83-3; MC1 (y = 1, z = 3, R = Me, R′ = Et), 130805-80-0; MC1 (y = z = 3, R = Me, R′ = Et) (homopolymer), 130805-81-1; MC2, 133985-23-6; MC2 (homopolymer), 133985-25-8; BuOH, 71-36-3; $Br(CH_2)_5COCl$, 22809-37-6; $MeN(Ph)(CH_2)_5CO_2Bu$, 120654-33-3; MeNPh, 100-61-8; $MeN(Ph)CH_2CO_2Et$, 21911-74-0; $BuN(Ph)CH_2CO_2Et$, 133985-21-4; $ClCH_2CO_2Et$, 105-39-5; $BrCH_2CO_2Et$, 105-36-2; $H_2NC_6H_4$-p-$S(CH_2)_6OH$, 131110-18-4; $H_2NC_6H_4$-p-$S(CH_2)_6OAc$, 131110-19-5; $H_2NC_6H_4$-p-SH, 1193-02-8; $Cl(CH_2)_6OH$, 2009-83-8; Ac_2O, 108-24-7; $H_2NC_6H_4$-p-$SO_2(CH_2)_6OH$, 131110-20-8; H_3CCO_2H, 64-19-7; $AcNHC_6H_4$-p-$SO_2(CH_2)_2CO_2Et$, 100610-78-4; $AcNHC_6H_4$-p-SO_2H·Na, 15898-43-8; $H_2NC_6H_4$-p-$SO_2(CH_2)_2CO_2Et$, 133985-22-5; $H_2NC_6H_4$-p-$SO_2(CH_2)_3OH$, 131110-21-9; $Br(CH_2)_5CO_2Bu$, 84970-50-3; BuNHPh, 1126-78-9; $H_2C{=}CHCO_2Et$, 140-88-5; $(H_2C{=}CHCH_2)_2NC_6H_4$-p-N=N-C_6H_4-p-SO_2Me, 133985-24-7.